

Model Predictive Direct Torque Control of Permanent Magnet Synchronous Motors

Tobias Geyer, *Member, IEEE*, Giovanni A. Beccuti, *Member, IEEE*,
Georgios Papafotiou, *Member, IEEE* and Manfred Morari, *Fellow, IEEE*

Abstract—Model Predictive Direct Torque Control (MPDTC) is a recent computational control methodology that combines the merits of Model Predictive Control (MPC) with the ones of Direct Torque Control (DTC). Specifically, with respect to standard DTC, the converter’s switching frequency and/or losses are considerably reduced, while at the same time the Total Harmonic Distortion (THD) levels of the phase currents and the torque are improved. Moreover, DTC’s favorable dynamic and robustness properties are preserved. This paper presents an MPDTC scheme for a permanent magnet synchronous motor that achieves long prediction horizons in the range of up to 150 time-steps through the use of extrapolation and bounds. A discrete-time internal controller model of the drive system is derived from the physical equations. Simulation results for a three-level voltage source inverter indicate that such an MPDTC scheme, compared to an industry standard controller, is capable of reducing the switching losses and the switching frequency by up to 50%, and the torque THD by 25%, while leaving the current THD unchanged.

Index Terms—Model predictive control, direct torque control, permanent magnet synchronous machine, medium-voltage drive

I. INTRODUCTION

One of the classical methods for controlling electrical motors is Direct Torque Control (DTC), initially introduced in [1] for induction motors [2], [3] and successively also for other configurations [4] such as synchronous machines [5], especially in the case of the permanent magnet type [6], [7]. The key notion behind DTC is to directly steer the stator flux vector by applying the appropriate voltage vector to the stator windings. This is done by using a pre-designed switching table to directly update the inverter’s discrete switch positions whenever the variables to be controlled, the electromagnetic torque and the stator flux, exceed the hysteresis bounds around their references. The switching table is derived on the basis of the desired performance specifications on the controlled variables, which, in the case of a three-level inverter, also include the balancing of the inverter’s neutral point potential around zero.

The success of DTC is closely associated with the performance advantages it brings with respect to the rapid and precise dynamic torque response. Furthermore, since the look-up table directly sets the switch positions of the semiconductor

components in the inverter, a pulse width or space vector modulator is not required. This however also implies a variable switching frequency, which is intrinsically connected with the width of the hysteresis bounds being used – more stringent bounds correspond to a higher switching frequency and vice versa. It is usually desirable to minimize the average switching frequency of the inverter, since this represents a rough measure of its switching losses and therefore of its energetic and economic cost, but in general DTC in itself cannot directly regulate or minimize the switching frequency and it might furthermore feature a relatively significant ripple on the current and torque.

To obviate these shortcomings different approaches have been reported in the literature, focusing mostly on drives with induction motors, as these represent the electrical motors most commonly employed in industrial applications [8], [9]. These approaches seek to ameliorate the design procedure of the switching table by improving the achievable trade-off between the switching frequency and the torque and flux ripple, by reducing the average inverter switching frequency for a given torque and flux ripple. The aforementioned methods however, although apt at being applied for two-level inverters, are not easily extendable to multi-level inverters [10].

The recent past has witnessed the formulation of a number of Model Predictive Control (MPC) based schemes for motor drives, partly as originally outlined in [11] and as presented for example in [12], where the latter actually refers to a synchronous motor setup. More specifically for permanent magnet (PM) motors MPC methods have also been presented featuring both modulation and DTC approaches. Examples of the former include [13], where the resulting continuous variable problem is tackled via an explicit solution approach, and [14], where a predictive scheme for operation in overmodulation is used to account and compensate for current distortions. Among the latter one has [15], [16] where a current control scheme was developed and experimentally evaluated against a classical DTC approach, and although the resulting comparison is favorable the issue of switching frequency reduction is not directly addressed.

It was specifically in relation to switching frequency issues that a novel model predictive control approach to the DTC problem was developed in [17], [18] for the three-phase induction motor, with the aim of regulating the system values within their imposed bounds whilst minimizing the resulting inverter switching frequency. The Model Predictive DTC (MPDTC) method featured therein is independent of the drive’s physical parameters and structural characteristics, so

T. Geyer is currently with the Department of Electrical and Computer Engineering, The University of Auckland, New Zealand; e-mail: t.geyer@ieee.org
A. G. Beccuti and G. Papafotiou are with ABB Corporate Research, Baden-Dättwil, Switzerland; e-mails: giovanni.beccuti@ch.abb.com, georgios.papafotiou@ch.abb.com

M. Morari is with the Automatic Control Laboratory, Department of Information Technology and Electrical Engineering, ETH Zurich, Zurich, Switzerland; e-mail: morari@ethz.ch

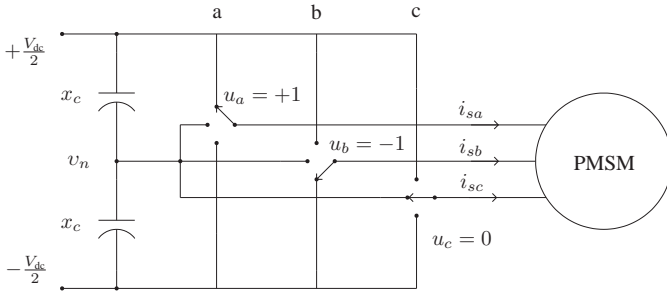


Fig. 1: Equivalent representation of a three-phase three-level voltage source inverter driving a permanent magnet synchronous motor

that the design procedure can be readily extended to other topologies. The initial MPDTC algorithm is available in two forms with switching horizons of one or two steps [17], [18]. Linear and quadratic extrapolation is used to achieve prediction horizons in the range of a couple of dozen steps. MPDTC was generalized in [19] allowing for an extended switching horizon, which is composed of multiple hinges (groups of switch transitions) linked by several extrapolation or extension segments. Moreover, the switching losses can be captured in the controller's objective function and thus directly minimized. The benefit of these two concepts is a further decrease in the switching losses. MPDTC's associated implementation complexity is within reach of existing controller hardware, as the experimental results presented in [20] confirm. It is specifically in view of these advantageous features in terms of performance, flexibility and technological viability that the same MPC approach has been investigated for and applied to the PM synchronous motor drive, as featured herein.

The present paper is structured as follows: Section II describes the physical drive system and the employed formalism, while the associated control problem and MPC concept are briefly resumed in Sections III-A and III-B. Section III-C presents the control model employed for the prediction of the drive system's behavior, and Section III-D presents the generalized MPDTC concept with its combination of switching hinges and extrapolation segments. In Section IV simulations for steady state operation are presented and compared with those of an industry standard controller, and lastly conclusions are drawn in Section V.

II. DRIVE SYSTEM

All variables and parameters in this paper are normalized using the per unit (pu) system. Accordingly, we will use the normalized time scale t with one time unit corresponding to $1/\omega_b$ seconds, where ω_b is the base angular velocity. Additionally, we will use $\xi(t)$, $t \in \mathbb{R}$, to denote continuous-time variables, and $\xi(k)$, $k \in \mathbb{N}$, to denote discrete-time variables with the sampling interval $T_s = 25 \mu\text{s}$. Often, when the dependency of ξ is apparent, we will simply write ξ to simplify the exposition.

A. The Three-Level Voltage Source Inverter

A schematic depiction of a three-phase three-level voltage source inverter connected to a PM synchronous motor is presented in Fig. 1. At each phase, the inverter can yield the

three distinct voltage levels $\{\frac{V_{dc}}{2}, 0, -\frac{V_{dc}}{2}\}$, where V_{dc} denotes the total dc-link voltage. The inverter's phase switch positions can be described through the integer variables $u_a, u_b, u_c \in \{1, 0, -1\}$, where $\{1, 0, -1\}$ respectively correspond to the voltages $\{\frac{V_{dc}}{2}, 0, -\frac{V_{dc}}{2}\}$. The vector of inverter switch positions can be written as

$$u_{abc} = [u_a \ u_b \ u_c]^T \in \{-1, 0, 1\}^3. \quad (1)$$

For a three-level voltage source inverter, the neutral point potential v_n deserves particular attention. According to [17] the continuous-time behavior of the neutral point potential is determined by

$$\frac{dv_n}{dt} = -\frac{1}{2x_c} \left((1 - |u_a|)i_{sa} + (1 - |u_b|)i_{sb} + (1 - |u_c|)i_{sc} \right), \quad (2)$$

where i_{sa}, i_{sb}, i_{sc} are the phase stator currents and x_c is the value of one of the two identical capacitors constituting the dc-link. By considering that $i_{sa} + i_{sb} + i_{sc} = 0$ it can be easily derived that

$$\frac{dv_n}{dt} = \frac{1}{2x_c} (|u_{abc}|^T i_{s,abc}) \quad (3)$$

where $|u_{abc}| = [|u_a| |u_b| |u_c|]^T$ denotes the componentwise absolute value of the inverter switch positions and $i_{s,abc} = [i_{sa} \ i_{sb} \ i_{sc}]^T$.

Additional constraints on the admissible switch transitions appear in conjunction with the design of the inverter, namely the installation of only one di/dt snubber in the upper and the lower inverter half, respectively. Specifically, each phase leg can switch only by at most one step, at most two phase legs can switch at the same time and if so, switching needs to occur in the opposite halves of the inverter. For example, from $[1 \ 1 \ 1]^T$, switching is only admissible to $[0 \ 1 \ 1]^T$, $[1 \ 0 \ 1]^T$ or $[1 \ 1 \ 0]^T$ (and not to any of the other 23 switch positions).

Switching losses arise in the inverter when turning the semiconductors on or off and commutating the phase current. These losses depend on the applied voltage, the commutated current and the semiconductor characteristics. Considering Integrated Gate Commutated Thyristors (IGCT), with the GCT being the semiconductor switch, the switch-on and switch-off losses can be well approximated to be linear in the dc-link voltage and the phase current. For diodes, the reverse recovery losses are again linear in the voltage, but nonlinear in the commutated current. As shown in [19], [21], for a given inverter topology, the switching losses can be derived as a function of the switching transition, the commutated phase current and its polarity.

B. The dq0 Reference Frame

The dynamical equations of the PM synchronous motor are conveniently expressed in an orthogonal coordinate system rotating synchronously with the machine's electrical field. Specifically, a $dq0$ reference frame is used. The physical three-phase abc values $\xi_{abc} = [\xi_a \ \xi_b \ \xi_c]^T$ are translated to $\xi_{dq0} = [\xi_d \ \xi_q \ \xi_0]^T$ in the $dq0$ frame through

$$\xi_{dq0} = P(\varphi_r) \xi_{abc}, \quad (4)$$

where φ_r denotes the angle between the a -axis of the three-phase system and the d -axis of the reference frame. By aligning the d -axis with the motor's rotor flux, φ_r also corresponds to the rotor's angular position. The transformation matrix is given by

$$P(\varphi_r) = \frac{2}{3} \begin{bmatrix} \cos(\varphi_r) & \cos(\varphi_r - \frac{2\pi}{3}) & \cos(\varphi_r + \frac{2\pi}{3}) \\ -\sin(\varphi_r) & -\sin(\varphi_r - \frac{2\pi}{3}) & -\sin(\varphi_r + \frac{2\pi}{3}) \\ \frac{1}{2} & \frac{1}{2} & \frac{1}{2} \end{bmatrix}. \quad (5)$$

The reference frame rotates with the angular speed $\omega_{fr} = \omega_r = \frac{d\varphi_r}{dt}$, where ω_r is the rotor's angular speed.

When modelling electrical machines, the 0-component of ξ_{dq0} is typically not required. For this, we introduce the transformation matrix $\tilde{P}(\varphi)$ that features the first two rows of $P(\varphi)$ only and yields

$$\xi_{dq} = [\xi_d \ \xi_q]^T = \tilde{P}(\varphi_r) \xi_{abc}. \quad (6)$$

C. The Permanent Magnet Synchronous Motor

A permanent magnet is mounted on the rotor of the synchronous machine that yields the associated constant magnetic flux linkage per second

$$\psi_{r,dq} = \begin{bmatrix} \psi_{rd} \\ \psi_{rq} \end{bmatrix} = \begin{bmatrix} \psi_{PM} \\ 0 \end{bmatrix}. \quad (7)$$

The stator flux linkage per second is given by

$$\psi_{s,dq} = X_s i_{s,dq} + \psi_{r,dq}, \quad (8)$$

with the stator self reactance

$$X_s = \begin{bmatrix} x_{ls} + x_{md} & 0 \\ 0 & x_{ls} + x_{mq} \end{bmatrix}. \quad (9)$$

In here, x_{ls} denotes the stator leakage reactance, and x_{md} and x_{mq} are the direct and quadrature axis magnetizing reactances, respectively. As well as $\psi_{r,dq}$, the stator flux linkage $\psi_{s,dq}$ and the stator current $i_{s,dq}$ are vectors with corresponding d - and q -components.

The voltage equation in dq is

$$v_{s,dq} = r_s i_{s,dq} + \frac{d}{dt} \psi_{s,dq} + \omega_r \begin{bmatrix} 0 & -1 \\ 1 & 0 \end{bmatrix} \psi_{s,dq}, \quad (10)$$

where $v_{s,dq}$ is the stator voltage vector in dq , and r_s the stator resistance. The former is the inverter voltage applied to the stator represented in the dq reference frame.

$$v_{s,dq} = \begin{bmatrix} v_{sd} \\ v_{sq} \end{bmatrix} = \frac{V_{dc}}{2} \tilde{P}(\varphi_r) u_{abc} \quad (11)$$

The electromagnetic torque is given by

$$T_e = \psi_{sd} i_{sq} - \psi_{sq} i_{sd}, \quad (12)$$

or equivalently by

$$T_e = \frac{1}{x_{ls} + x_{md}} \left(\frac{x_{md} - x_{mq}}{x_{ls} + x_{mq}} \psi_{sd} + \psi_{rd} \right) \psi_{sq}, \quad (13)$$

where the latter equation can be derived by solving (8) for $i_{s,dq}$ and substituting it in (12). Note that due to the saliency of the machine, the torque is also a function of the d -component of the stator flux, albeit to a small degree only. The magnitude of the stator flux is obtained through

$$\Psi_s = \sqrt{\psi_{sd}^2 + \psi_{sq}^2}. \quad (14)$$

Notice that both expressions are effectively nonlinear functions of the flux vector components. The voltage equation (10) along with (7)-(9) and (11) represent a standard dynamical formulation of the synchronous motor, and alongside the inverter equation (3), it constitutes the starting point of the internal controller model to be developed in Section III-C.

The motor dynamics can be distinguished into two groups with regards to their time constants. The mechanical part, i.e. the rotational speed dynamic, which is not shown here, is slow as it evolves within a lapse of a few seconds, whereas the stator flux exhibits considerably faster dynamics, which can be manoeuvred by the applied inverter voltage in a matter of several microseconds.

III. CONTROL SCHEME

A. Control Problem and Objectives

The control problem includes objectives regarding both the motor and the inverter. First and foremost for the motor, the electromechanical torque T_e delivered at the shaft must be kept close to its reference $T_{e,ref}$ by maintaining it between the lower and upper limit values $T_{e,min}$ and $T_{e,max}$. The torque reference is either directly set by the user or by an external speed control loop. Secondly, in order to avert motor saturation or demagnetization, the magnitude of the stator flux Ψ_s must be kept between the given bounds $\Psi_{s,min}$ and $\Psi_{s,max}$. The main control objective relating to the inverter operation consists in minimizing the average switching frequency (and/or the switching losses) on the inverter legs, and additionally keeping the inverter's neutral point potential v_n within the limits $v_{n,min}$ and $v_{n,max}$ around zero.

B. Model Predictive Control

The algorithmic concept of Model Predictive DTC (MPDTC) is based on the principles of constrained optimal control, specifically Model Predictive Control (MPC). MPC has been traditionally and successfully employed in a variety of industrial applications and has more recently been the object of study and investigation in the fields of power electronics and drives. This is directly related to the fact that it is a systematic control method allowing one to deal with complex, multi-variable systems subject to constraints by directly formulating a discrete-time control model of the plant. The desired control objectives are replicated in an appropriately selected cost function mirroring the order of importance of the imposed objectives. At each sampling instant the control action is obtained by minimizing the cost function over a prediction horizon subject to the equations and constraints of the model. The first control input in the optimal input sequence is then applied to the system and the procedure is repeated at the

successive sampling instant. Further details about MPC can be found in [22].

C. Internal Controller Model

For the formulation of the optimal control problem, a discrete-time model of the drive system is needed to serve as internal controller model. The sampling period T_s is employed, with the discrete-time step k corresponding to the time-instant kT_s . Since T_s is typically $25 \mu\text{s}$ and the prediction horizon is in the range of a few 100 steps, or equivalently a few ms, the rotor speed within the prediction interval can be assumed to be constant. Therefore, a dynamical equation describing the rotor speed evolution within the prediction interval is not required, and the rotor speed can be considered to be a parameter. To be precise, the rotor speed is a time-varying parameter in the controller model, implying that the model equations need to be updated as the rotor speed varies.

Solving (8) for $i_{s,dq}$ and substituting it into the motor's voltage equation (11) yields

$$\frac{d}{dt}\psi_{s,dq}(t) = (F_r - F_m)\psi_{s,dq}(t) + F_m\psi_{r,dq} + v_{s,dq}(t) \quad (15)$$

with the matrices

$$F_m = \begin{bmatrix} \frac{r_s}{x_{ls}+x_{md}} & 0 \\ 0 & \frac{r_s}{x_{ls}+x_{mq}} \end{bmatrix}, \quad F_r = \begin{bmatrix} 0 & \omega_r \\ -\omega_r & 0 \end{bmatrix}. \quad (16)$$

Due to the rotation of the dq reference frame, the stator voltage expressed in the dq frame, i.e. $v_{s,dq}$, is time-varying even when u_{abc} remains constant. This is also the case during the sampling interval and will complicate the derivation of the discrete-time model.

The discrete-time linear motor model is obtained by integrating (15) from $t = kT_s$ to $t = (k+1)T_s$ which yields

$$\begin{aligned} \psi_{s,dq}((k+1)T_s) &= e^{(F_r-F_m)T_s}\psi_{s,dq}(kT_s) \\ &+ F_m \int_0^{T_s} e^{(F_r-F_m)(T_s-\tau)} d\tau \psi_{r,dq} \\ &+ \frac{V_{dc}}{2} \int_0^{T_s} e^{(F_r-F_m)(T_s-\tau)} \tilde{P}(\varphi_r(kT_s+\tau)) u_{abc}(kT_s+\tau) d\tau. \end{aligned} \quad (17)$$

In the following, we focus on the third expression on the right-hand side of (17), which can be simplified using the following three relations. Firstly, as the componentwise product between F_m and F_r is zero, one can write

$$e^{(F_r-F_m)(T_s-\tau)} = e^{F_r(T_s-\tau)} e^{F_m(\tau-T_s)}. \quad (18)$$

Secondly, since $\varphi_r(kT_s+\tau) = \varphi_r(k) + \omega_r\tau$, the relation

$$e^{-F_r\tau} \tilde{P}(\varphi_r(kT_s+\tau)) = \tilde{P}(\varphi_r(kT_s)) \quad (19)$$

can be shown to hold. Moreover, it is straightforward to derive

$$e^{F_r T_s} \tilde{P}(\varphi_r(kT_s)) = \tilde{P}(\varphi_r(kT_s) + \omega_r T_s). \quad (20)$$

Using (18), (19) and (20), and recalling that the voltage vector applied to the motor terminals remains constant within one

sampling interval we can rewrite the third expression in (17) as

$$\frac{V_{dc}}{2} \int_0^{T_s} e^{F_m(\tau-T_s)} d\tau \tilde{P}(\varphi_r(kT_s) + \omega_r T_s) u_{abc}(kT_s). \quad (21)$$

In a last step, the integrals in (17) and (21) are solved to obtain the discrete-time motor model in the compact form

$$\begin{aligned} \psi_{s,dq}(k+1) &= A\psi_{s,dq}(k) + B_1\psi_{r,dq} \\ &+ \frac{V_{dc}}{2} B_2 \tilde{P}(\varphi_r(k) + \omega_r T_s) u_{abc}(k), \end{aligned} \quad (22)$$

where we have used k rather than kT_s to denote the sampling instants, and introduced the matrices

$$A = e^{(F_r-F_m)T_s} \quad (23a)$$

$$B_1 = -F_m(F_r - F_m)^{-1}(I_2 - A) \quad (23b)$$

$$B_2 = F_m^{-1}(I_2 - e^{-F_m T_s}) \quad (23c)$$

with I_2 being the two-dimensional identity matrix.

The evolution of the angular position can be trivially captured via

$$\varphi_r(k+1) = \varphi_r(k) + \omega_r T_s. \quad (24)$$

For the neutral point a less precise discretization method suffices – starting from (3) and using a forward Euler approach one obtains

$$v_n(k+1) = v_n(k) + \frac{1}{2x_c} (|u_{abc}(k)|^T i_{s,abc}(k)) T_s, \quad (25)$$

where the stator currents $i_{s,abc}$ can be expressed as a function of the motor fluxes and the angular position through

$$i_{s,abc}(k) = \tilde{P}(\varphi_r(k))^{-1} X_s^{-1} (\psi_{s,dq}(k) - \psi_{r,dq}). \quad (26)$$

In this model the stator currents are only needed to compute the evolution of the neutral point potential using (25) and to derive the predicted switching losses according to Section II-A. Since accuracy is for both not that critical one might assume the stator currents to be constant within the prediction horizon so as to reduce the computational burden associated with the internal controller model.

Recapitulating the above, the internal controller model has the state vector

$$x(k) = [\psi_{sd}(k) \ \psi_{sq}(k) \ \varphi_r(k) \ v_n(k)]^T \quad (27)$$

and the output vector

$$y(k) = [T_e(k) \ \Psi_s(k) \ v_n(k)]^T. \quad (28)$$

Using (13) and (14) the output vector $y(k)$ can be directly written as a nonlinear function of $x(k)$.

D. Model Predictive Direct Torque Control

Recall that the MPDTC objective is to minimize the switching frequency (or the switching losses) while keeping the controlled variables y , i.e. the torque, stator flux magnitude and neutral point potential, within their given bounds. The combination of a short sampling interval of usually $25 \mu\text{s}$ and a switching frequency that is typically in the range of a few hundred Hertz for medium-voltage applications,

requires very long prediction horizons of hundreds of time-steps to capture the evolution of the switching frequency in the controller's objective function. To avoid the associated explosion in computational complexity due to the model's switching characteristics, a short switching horizon is used in connection with a long prediction horizon.

1) *Original MPDTC Algorithm:* In the original MPDTC formulation described in [17], [18] and shown in Fig. 2, the switch position $u(k)$, i.e. the control input, is determined at each sampling instant kT_s as follows. Starting from the previously applied switch position $u(k-1)$, the admissible inverter switching sequences are enumerated over a short switching horizon of length N_s . The switching sequences can be considered as a sequence of control actions over the control horizon. By applying each switching sequence to the discrete-time internal controller model a corresponding predicted output trajectory $[y(k+1), \dots, y(k+N_s)]$ is obtained.

Next, the so called *candidate* switching sequences are determined. These are switching sequences that yield output trajectories that are either feasible at the end of the switching horizon (the output variables lie within their respective bounds) or, if they are outside their bounds, progressively reduce the degree of the bound's violation. To achieve a long prediction horizon N_p the output trajectories referring to candidate trajectories are extrapolated in time and the number of time-steps is determined for which the output variables are kept within their bounds.

Linear extrapolation is computationally very cheap and it is this crucial aspect that renders the overall approach viable even if the switching horizon N_s is short. The cost associated with each switching sequence is computed by dividing the total number of switch transitions in the sequence by the length (number of time-steps) of the associated extrapolated trajectory. This yields a predicted short-term switching frequency.

An input with low cost, that is an input which requires few switch transitions and keeps the outputs feasible for a long interval, is intuitively a good choice in terms of both the switching frequency and the resulting ripple, so that minimizing this value is the criterion through which the optimal switching sequence is chosen. Out of this sequence, only the first element, the switch position $u(k)$, is applied to the inverter.

2) *Generalized MPDTC Algorithm:* As introduced in [19] the above formulation can be generalized by considering longer switching horizons with multiple switching instants and extrapolation segments. Moreover, the switching losses can be included in the controller model and directly minimized rather than indirectly via the switching frequency, as also proposed in [21].

Starting at the current time-step k , the generalized MPDTC algorithm iteratively explores the tree of feasible switching sequences forward in time. At each intermediate step, all switching sequences must remain candidate sequences – otherwise they are being discarded. The traversing through the tree is controlled by the so called *switching horizon* composed of the elements 'S' and 'E', which stand for 'switch' and 'extrapolate' (or more generally 'extend'), respectively. The

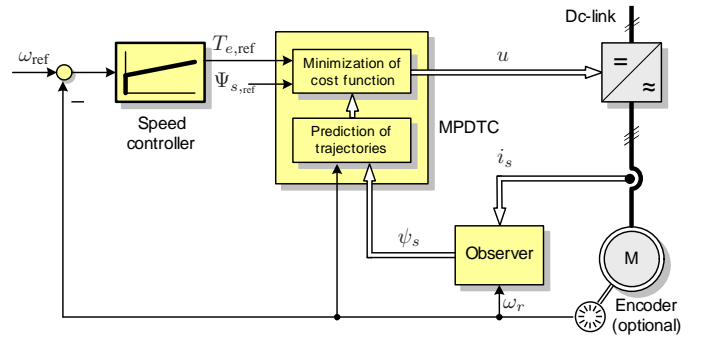


Fig. 2: Schematic of model predictive direct torque control (MPDTC) for a voltage source inverter driving a permanent magnet synchronous machine

switching horizon can be considered as an alternative to a horizon of fixed length. Note that for MPDTC, the resulting prediction horizon N_p is of variable length. As an example for a switching horizon, consider 'SSESE', which stands for switching at time-steps k and $k+1$ and subsequently extending the trajectories until one or more output trajectory ceases to be feasible and/or pointing in the proper direction. Assume this happens at time-step $k+l$ thus triggering the third switching event that is followed by another extension step. We use the task 'e' to add an optional extension leg to the switching horizon.

Using 'eSSESE' as an example, one candidate switching sequence is depicted in Fig. 3 along with its corresponding output trajectories. Starting at the present time-step k , after an (optional) extrapolation step 'e', the phases b and c switch at time-step $k+37$, while at step $k+38$ phase a switches. These transitions constitute the first two switching events 'SS' in the horizon. Note that these switching transitions cannot occur at the same time due to the snubber constraint. At time-step $k+49$ the phases b and c switch again followed by another extrapolation segment.

At time-step k , the generalized MPDTC algorithm computes $u(k)$ according to the following procedure [19].

- 1) Initialize the root node with the current state vector $x(k)$, the last switch position $u(k-1)$ and the switching horizon. Push the root node onto the stack.
- 2a) Take the top node with a non-empty switching horizon from the stack.
- 2b) Read out the first element. For 'S', branch on all admissible switch transitions according to Section II-A. For 'E', extend the trajectories either by extrapolation as detailed in [17] or by using the internal controller model derived in Section III-C.
- 2c) Keep only the switching sequences that are candidates.
- 2d) Push these sequences onto the stack.
- 2e) Stop if there are no more nodes on the stack with non-empty switching horizons. The result of this are the predicted (candidate) switching sequences $U^i(k) = [u^i(k), \dots, u^i(k+n_i-1)]$ of length n_i , where $i \in \mathcal{I}$ and \mathcal{I} is an index set.
- 3) Compute for each (candidate) sequence $i \in \mathcal{I}$ the associated cost. If the switching frequency is to be minimized, consider $c_i = s_i/n_i$, which approximates the average

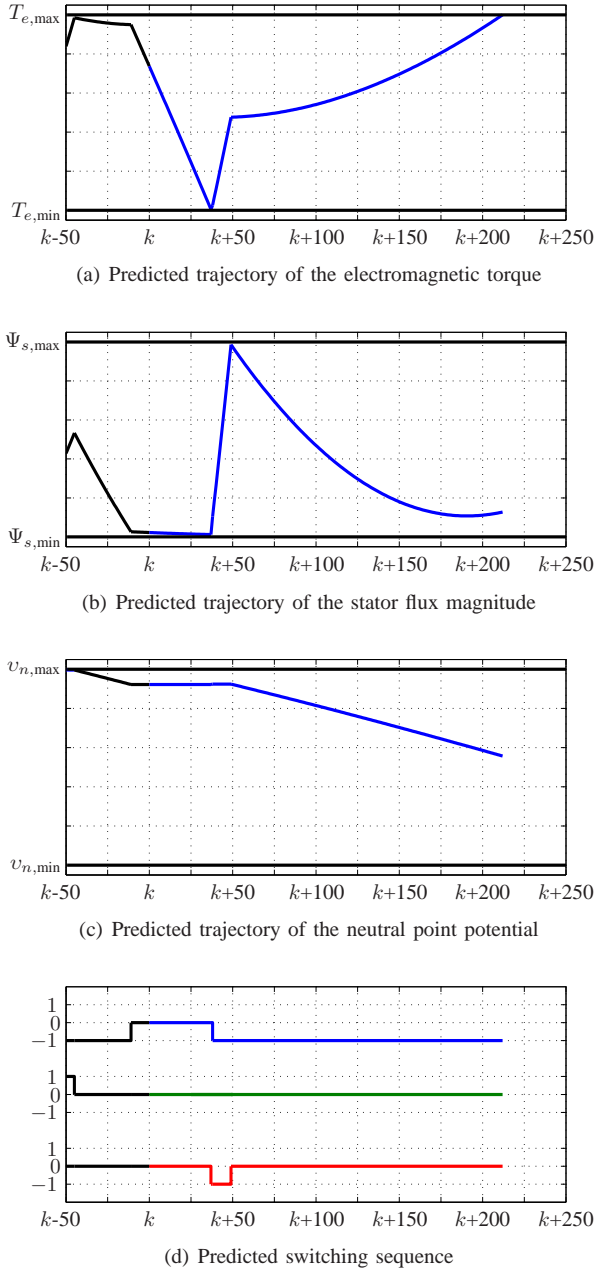


Fig. 3: Candidate switching sequence with the associated torque, stator flux and neutral point trajectories between their respective upper and lower bounds. The time-axis is given by the sampling instants with the sampling interval $T_s = 25 \mu\text{s}$. The switching horizon 'eSSESE' leads here to a prediction horizon of $N_p = 213$ time-steps or 5.325 ms.

switching frequency, where $s_i = \sum_{\ell=k}^{k+n_i-1} \|u_i(\ell) - u_i(\ell-1)\|_1$ is the total number of switch transitions in the switching sequence $U^i(k)$. Conversely, if the switching losses are targeted, the cost function $c_i = E_i/n_i$ is used, where E_i is the sum of the switching (energy) losses according to Section II-A.

- 4) Choose the switching sequence $U^* = U^i(k)$ with the minimal cost, where $i = \arg \min_{i \in \mathcal{I}} c_i$.
- 5) Apply (only) the first switch position $u(k) = u^*$ of this sequence and execute the above procedure again at the next time-step $k+1$.

PM Synchronous Motor			
Rated voltage	3000 V	x_{md}	0.550 pu
Rated current	328 A	x_{mq}	0.481 pu
Apparent power	1.704 MVA	x_{ls}	0.275 pu
Rated frequency	16 Hz	r_s	0.030 pu
Rated speed	80 rpm	ψ_{rd}	1.110 pu
Inverter			
Dc-link voltage	4294 V	V_{dc}	1.753 pu
		x_c	3.716 pu

TABLE I: Rated values (left) and parameters (right) of the permanent magnet synchronous motor and inverter

Note that the prediction horizon induced by the switching horizon is given by $N_p = \max_{i \in \mathcal{I}}(n_i)$.

IV. PERFORMANCE EVALUATION

In the following, for a PM synchronous machine whose ratings and parameters are summarized in Table I, MPDTC's performance at steady-state is compared with the one of standard DTC. The comparison is done in terms of the switching losses P_{sw} , the switching frequency f_{sw} , and the current and torque THDs $I_{s,THD}$ and $T_{e,THD}$, respectively. Standard DTC is used as the baseline. The operating point is at 80% speed and 100% torque. The width of the bounds, given by the upper minus the lower bound, is always 5% for the neutral point potential.

Three comparisons between DTC and MPDTC are shown hereafter. The first comparison is based on using effectively the same bounds on the torque, stator flux and neutral point, the second one focuses on the same current THD, while the third comparison maintains the same switching losses. The related results are shown in Tables II, III and IV, respectively. In these comparisons, the impact of the length of the switching horizon with a varying number of switching hinges and extrapolation blocks is demonstrated. Moreover, the controller's objective is altered between minimizing the switching frequency and the losses. The resulting average prediction horizons are also shown.

In the first comparison, MPDTC's torque and flux bounds were slightly widened to account for DTC's bound violations, namely a bound width of 6% was used for the torque, 3.3% for the stator flux and 5% for the neutral point potential. Table II illustrates that there is a clear benefit in directly reducing either the switching losses or the switching frequency, with a maximum decrease of the targeted quantities of about 50% when using long horizons. The current distortion is increased in some cases, but more importantly the torque THD is reduced.

Figs. 4 and 5 depict system values during steady-state operation at 80% speed and 100% torque for the cases corresponding to the first and last rows of Table II, i.e. standard DTC vs. MPDTC with 'eSSESE' employing switching frequency minimization. Even though the bounds were slightly widened in MPDTC to account for the intermittent violations in DTC, the obtained torque and flux ripples are smaller. Most importantly, the switching frequency is more than halved when compared to DTC.

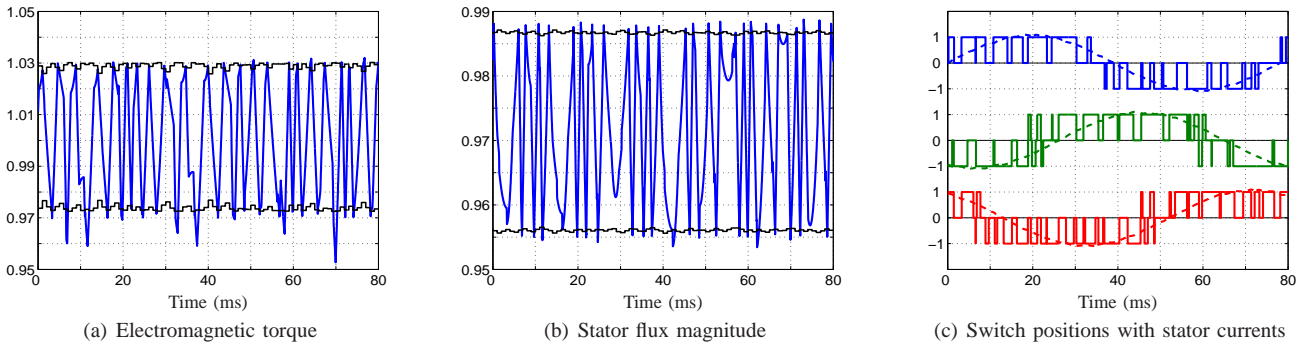


Fig. 4: Standard DTC corresponding to the first rows in Tables II, III and IV. All signals are given in pu.

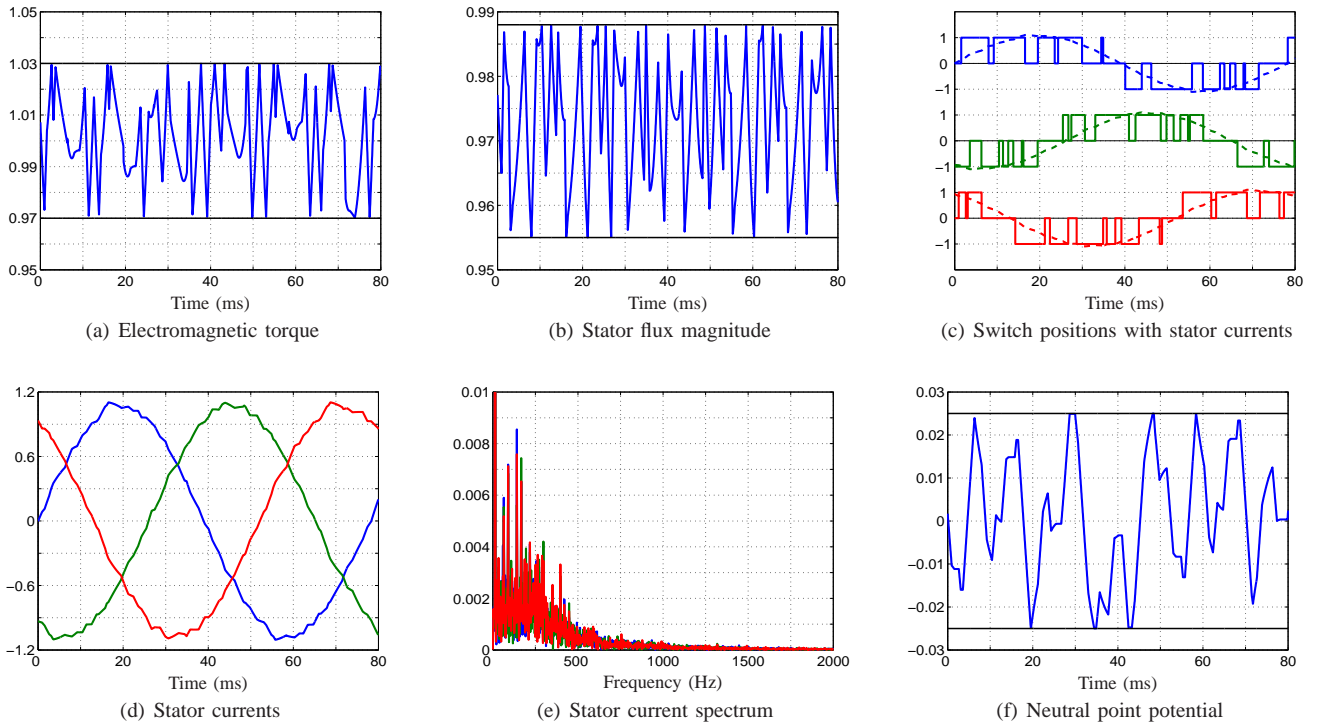


Fig. 5: MPDTC with the switching horizon 'eSSESESE' minimizing the switching frequency, and corresponding to the last row in Table II. The operating point and the scaling are the same as in Fig. 4 to facilitate a direct comparison. The torque and flux bounds were slightly widened to account for DTC's violations of the bounds. All signals are given in pu.

In the second comparison, the torque and flux bounds are modified in MPDTC so as to achieve similar current distortion levels as in DTC. As displayed in Table III the switching frequency and losses are again improved by up to 50%, both in the case where they are directly minimized and also when the controller tries to curb the switching frequency. Notice that the reverse does not necessarily hold, at least not to the same extent, as it is possible to reduce the switching losses despite switching relatively often by switching predominantly when the phase currents and thus the losses are low.

This fact can be also observed from the results of the third comparison, in which the switching losses are kept constant, and the torque and flux bounds are adjusted accordingly for MPDTC. Specifically, in the second column of Table IV, for the same losses the switching frequency is clearly higher when

it is not explicitly minimized. Of greater interest, however, is the fact that the current and torque distortion levels are distinctly lower than those of standard DTC. The current THD is reduced by one third, while the torque THD is reduced by two thirds and more, when keeping the switching losses unchanged.

The performance in terms of the switching losses and the switching frequency generally improves for the overall simulations as the number of switching instants and extrapolation segments is increased in the horizon. Specifically, MPDTC with the short switching horizon 'eSSE' leads to a considerable degree of performance improvement when compared to standard DTC. Increasing the switching horizon from 'eSSE' to the long horizon 'eSSESESE' effectively doubles this performance improvement.

Control scheme	Switching horizon	Pred. horizon	Obj.	P_{sw} [%]	f_{sw} [%]	$I_{s,THD}$ [%]	$T_{e,THD}$ [%]
DTC	–	–	–	100	100	100	100
MPDTC	eSSE	40.5	P_{sw}	72.0	95.2	128	90.0
MPDTC	eSSESE	99.1	P_{sw}	52.6	69.9	119	88.1
MPDTC	eSSESESE	163	P_{sw}	46.6	63.7	116	85.1
MPDTC	eSSE	35.4	f_{sw}	103	95.2	117	84.1
MPDTC	eSSESE	103	f_{sw}	59.5	65.8	109	85.1
MPDTC	eSSESESE	167	f_{sw}	55.2	51.2	103	79.1

TABLE II: Performance comparison of MPDTC with standard DTC when using similar bounds. For MPDTC the switching horizons and the objective function (minimization of the switching frequency or the switching losses, respectively) are varied. DTC serves as the 100% baseline.

Control scheme	Switching horizon	Pred. horizon	Obj.	P_{sw} [%]	f_{sw} [%]	$I_{s,THD}$ [%]	$T_{e,THD}$ [%]
DTC	–	–	–	100	100	100	100
MPDTC	eSSE	34.3	P_{sw}	82.8	116	95.7	59.7
MPDTC	eSSESE	78.7	P_{sw}	67.7	86.3	102	65.7
MPDTC	eSSESESE	150	P_{sw}	48.3	63.0	96.1	69.7
MPDTC	eSSE	39.8	f_{sw}	80.2	78.8	94.8	62.7
MPDTC	eSSESE	83.9	f_{sw}	71.1	68.5	93.6	63.7
MPDTC	eSSESESE	161	f_{sw}	53.9	51.2	102	75.1

TABLE III: Performance comparison of MPDTC with standard DTC for a similar current distortion level

V. CONCLUSIONS

MPC offers an attractive and flexible way of dealing with complex control problems and has manifested itself in recent and promising applications in the area of power electronics and drives. This paper presented a model predictive direct torque control method for PM synchronous machines. As the presented numerical results for steady-state operation indicate long horizons lead to particularly promising performance results. Specifically, for a given current distortion level the switching frequency and the switching losses can be reduced by about 50%, when compared to industrial DTC. Vice versa, the switching frequency and losses are reduced by 40% for the same current THD. The torque THD can be reduced by up to 70% with respect to DTC. The dynamic behavior of MPDTC during transients such as torque steps is effectively the same as in DTC, as previous results in [20] indicate.

Future work will focus on corroborating the performed simulations through experimental validation. To enable the implementation of long switching horizons a recently proposed computationally efficient version of MPDTC can be considered that drastically reduces the computation time by using branch and bound techniques from mathematical programming [23].

REFERENCES

- [1] I. Takahashi and T. Noguchi. A new quick response and high efficiency control strategy for the induction motor. *IEEE Trans. Ind. Applicat.*, 22(2):820–827, Sep./Oct. 1986.
- [2] P. Pohjalainen, P. Tiitinen, and J. Lulu. The next generation motor control method - direct torque control, DTC. In *Proc. Eur. Power Electron. Chapter Symp.*, volume 1, pages 115–120, Lausanne, Switzerland, 1994.
- [3] I. Takahashi and Y. Ohmori. High-performance direct torque control of an induction motor. *IEEE Trans. Ind. Applicat.*, 25(2):257–264, Mar./Apr. 1989.

Control scheme	Switching horizon	Pred. horizon	Obj.	P_{sw} [%]	f_{sw} [%]	$I_{s,THD}$ [%]	$T_{e,THD}$ [%]
DTC	–	–	–	100	100	100	100
MPDTC	eSSE	27.9	P_{sw}	100	140	80.3	48.3
MPDTC	eSSESE	52.2	P_{sw}	100	134	64.8	27.4
MPDTC	eSSE	30.9	f_{sw}	101	107	78.1	49.8
MPDTC	eSSESE	60.5	f_{sw}	99.6	95.9	62.2	34.8

TABLE IV: Performance comparison of MPDTC with standard DTC for similar inverter switching losses

- [4] P. Vas. *Sensorless Vector and Direct Torque Control*. Oxford Univ. Press, 1998.
- [5] M. R. Zolghadri, D. Diallo, and D. Roje. Direct torque control system for synchronous machine. In *Proc. Eur. Conf. on Power Electron. and Applicat.*, pages 694–699, Trondheim, Norway, Sep. 1997.
- [6] L. Zhong, M. F. Rahman, W. Y. Hu, and K. W. Lim. Analysis of direct torque control in permanent magnet synchronous motor drives. *IEEE Trans. Power Electron.*, 12(3):528–536, May 1997.
- [7] M. F. Rahman, L. Zhong, and K. W. Lim. A direct torque controlled interior permanent magnet synchronous motor drive incorporating field weakening. *IEEE Trans. Ind. Applicat.*, 34(6):1246–1253, Nov./Dec. 1998.
- [8] D. Casadei, G. Serra, and A. Tanni. Implementation of a direct torque control algorithm for induction motors based on discrete space vector modulation. *IEEE Trans. Power Electron.*, 15(4):769–777, Jul. 2000.
- [9] A. Purcell and P. P. Acarnley. Enhanced inverter switching for fast response direct torque control. *IEEE Trans. Power Electron.*, 16(3):382–389, May 2001.
- [10] C. A. Martins, X. Roboam, T. Meynard, and A. Carvalho. Switching frequency imposition and ripple reduction in DTC drives by using a multilevel converter. *IEEE Trans. Power Electron.*, 17(2):286–297, Mar. 2002.
- [11] R. Kennel and A. Linder. Predictive control of inverter supplied electrical drives. In *Proc. IEEE Power Electron. Spec. Conf.*, volume 2, pages 761–766, Galway, Ireland, 2000.
- [12] J. M. Retif, X. Lin-Shi, A. M. Llor, and F. Morand. New hybrid direct-torque control for a winding rotor synchronous machine. In *Proc. IEEE Power Electron. Spec. Conf.*, volume 1, pages 1438–1442, Aachen, Germany, Jun. 2004.
- [13] S. Mariethoz, A. Domahidi, and M. Morari. Sensorless explicit model predictive control of permanent synchronous motors. In *Proc. IEEE Int. Electr. Mach. and Drive Conf.*, pages 1492–1499, Miami, Florida, USA, May 2009.
- [14] S. Matsutani, T. Zanma, K. Kawai, M. Ishida, A. Imura, and M. Fujit-suna. Optimal control of PMSMs using model predictive control. In *Proc. IEEE Ind. Electron.*, pages 1305–1310, Orlando, FL, Nov. 2008.
- [15] X. Lin-Shi, F. Morel, A. M. Llor, B. Allard, and J. M. Retif. Implementation of hybrid control for motor drives. *IEEE Trans. Ind. Electron.*, 54(4):1946–1952, Aug. 2007.
- [16] F. Morel, X. Lin-Shi, J. M. Retif, and B. Allard. A predictive current control applied to a permanent magnet synchronous machine, comparison with a classical direct torque control. *Electr. Power Syst. Res.*, 78(8):1437–1447, Aug. 2008.
- [17] T. Geyer. *Low Complexity Model Predictive Control in Power Electronics and Power Systems*. PhD thesis, Automatic Control Laboratory ETH Zurich, 2005.
- [18] T. Geyer, G. Papafotiou, and M. Morari. Model predictive direct torque control - part I: Concept, algorithm and analysis. *IEEE Trans. Ind. Electron.*, 56(6):1894–1905, Jun. 2009.
- [19] T. Geyer. Generalized model predictive direct torque control: Long prediction horizons and minimization of switching losses. In *Proc. IEEE Conf. on Decis. and Control*, Shanghai, China, Dec. 2009.
- [20] G. Papafotiou, J. Kley, K. G. Papadopoulos, P. Böhren, and M. Morari. Model predictive direct torque control - part II: Implementation and experimental evaluation. *IEEE Trans. Ind. Electron.*, 56(6):1906–1915, Jun. 2009.
- [21] S. Mastellone, G. Papafotiou, and E. Liakos. Model predictive direct torque control for MV drives with LC filters. In *Proc. Eur. Power Electron. Conf.*, Barcelona, Spain, Sep. 2009.
- [22] J. M. Maciejowski. *Predictive Control*. Prentice Hall, 2002.
- [23] T. Geyer. Computationally efficient model predictive direct torque control. In *Proc. IEEE Energy Conv. Congr. and Exp.*, Atlanta, USA, Sep. 2010.